



HAL
open science

Comparison of the dislocation density obtained by HR-EBSD and X-ray profile analysis

Szilvia Kalácska, Istvan Groma, András Borbély, Péter Dusán Ispánovity

► **To cite this version:**

Szilvia Kalácska, Istvan Groma, András Borbély, Péter Dusán Ispánovity. Comparison of the dislocation density obtained by HR-EBSD and X-ray profile analysis. *Applied Physics Letters*, 2017, 110 (Issue: 9), pp.Article Number : 091912. 10.1063/1.4977569 . emse-01593661

HAL Id: emse-01593661

<https://hal-emse.ccsd.cnrs.fr/emse-01593661v1>

Submitted on 8 Nov 2024

HAL is a multi-disciplinary open access archive for the deposit and dissemination of scientific research documents, whether they are published or not. The documents may come from teaching and research institutions in France or abroad, or from public or private research centers.

L'archive ouverte pluridisciplinaire **HAL**, est destinée au dépôt et à la diffusion de documents scientifiques de niveau recherche, publiés ou non, émanant des établissements d'enseignement et de recherche français ou étrangers, des laboratoires publics ou privés.

Comparison of the dislocation density obtained by HR-EBSD and X-ray profile analysis

Szilvia Kalácska,¹ István Groma,^{1,*} András Borbély,² and Péter Dusán Ispánovity¹

¹*Department of Materials Physics, Eötvös University Budapest, H-1517 Budapest POB 32, Hungary*

²*Ecole Nationale Supérieure des Mines, SMS-EMSE,*

CNRS:UMR 5307, LGF, 42023, Saint-Etienne Cedex 2, France

(Dated: October 28, 2016)

Based on the cross correlation analysis of the Kikuchi diffraction patterns high-resolution EBSD is a well established method to determine the internal stress in deformed crystalline materials. In many cases, however, the stress values obtained at the different scanning points have a large (in the order of GPa) scatter. As it was first demonstrated by Wilkinson and co-workers this is due to the long tail of the probability distribution of the internal stress ($P(\sigma)$) generated by the dislocations present in the system. According to the theoretical investigations of Groma and co-workers the tail of $P(\sigma)$ is inverse cubic with prefactor proportional to the total dislocation density $\langle \rho \rangle$. In this paper we present a direct comparison of the X-ray line broadening and $P(\sigma)$ obtained by EBSD on deformed Cu single crystals. It is shown that $\langle \rho \rangle$ can be determined from $P(\sigma)$. This opens new perspectives for the application of EBSD in determining mesoscale parameters in a heterogeneous sample.

Quantitative characterization of plastically deformed crystals in terms of dislocation density by transmission electron microscopy (TEM) and X-ray diffraction was a very important step in the development of basic models of crystal plasticity¹. This is especially true in the case of the composite model² of heterogeneous dislocation structures, which postulates Taylor type³ relations between the local flow stress and local dislocation density. Accessing local field quantities, however, requires methods capable to capture structural heterogeneities at the sub-micrometer scale, which can be done with the TEM, but obtaining statistically significant information necessitates a large amount of work. Development of novel automated characterization methods providing dislocation density data at the local scale is therefore important.

The aim of the present work is to present a new method for the evaluation of the average dislocation density at the mesoscale. It is based on the statistical properties of the distribution of local stresses determined by high-resolution backscatter electron diffraction (HR-EBSD)⁴. To address their physical significance, the results will be compared to the outcome of discrete dislocation dynamics simulations and X-ray diffraction (XRD) line profile analysis⁵. The latter is a well established experimental technique for determining microstructural parameters such as coherent domain size, dislocation density and its fluctuation. As shown by Groma *et. al.*⁵⁻⁸ in the so-called "strain broadening" setup⁵ the two leading terms of the asymptotic decay region of the intensity distribution $I(q)$ read as

$$I(q) = \frac{1}{\pi^2 d} \frac{1}{q^2} + \frac{\Lambda}{4\pi^2} \langle \rho \rangle \frac{1}{q^3} \quad |q| > q_0 \quad (1)$$

where $q = 2[\sin(\Theta) - \sin(\Theta_0)]/\lambda$, d is the coherent domain size, $\langle \rho \rangle$ is the average dislocation density and λ is the wavelength of the X-rays. Θ and Θ_0 are the half of the scattering angle and the Bragg angle, respectively. The parameter Λ is commonly given in the form

$\Lambda = 2|\vec{g}|^2|\vec{b}|^2C_g/\pi$ where \vec{b} and \vec{g} are the Burgers and the diffraction vector, respectively. C_g is called the *diffraction contrast factor* and depends on the type of the dislocation and the relative geometrical position between the dislocation line direction and the direction of \vec{g} . A detailed description of the contrast factor calculation can be found in⁷. A remarkable feature of Eq. (1) is its independence from the configuration of dislocations usually described in terms of dislocation-dislocation correlations. Certainly, the q_0 value from which Eq. (1) describes well the asymptotic region depends on correlations as it will be exemplified later. Considering that the tail of the experimental intensity curve can be rather noisy the actual values of the domain size and the dislocation density can be better obtained from the integral quantity

$$M_2(q) = \int_{-q}^q q'^2 I(q') dq' \quad (2)$$

called as second order restricted moment^{5,7}. Analyzing higher order restricted moments can also be useful^{6,7}, but for the experimental investigations presented here the use of $M_2(q)$ is enough. After substituting Eq. (1) into Eq. (2) at large enough q values we get

$$M_2(q) = \frac{1}{\pi^2 d} q + \frac{\Lambda}{2\pi^2} \langle \rho \rangle \ln \left(\frac{q}{q_0} \right) \quad (3)$$

where q_0 is a constant depending on the dislocation-dislocation correlation. If the coherent domain size is larger than of about $1 \mu\text{m}$ the first term in Eq. (3) becomes negligible beside the contribution of dislocations and the plot of M_2 versus $\ln(q)$ becomes a straight line in the asymptotic regime $q \rightarrow \infty$. Its slope is proportional to the mean dislocation density. Using this feature the dislocation density can be determined with an accuracy of a few percent.

HR-EBSD is a scanning electron microscope (SEM) based method, which allows determining the stress/strain

in a crystalline material at the length scale of tens of nanometers. It is based on a cross-correlation method^{4,9–14} exploiting small changes in backscattered Kikuchi diffraction patterns corresponding to reference point and the actual point analysed. A detailed description of the technique can be found in^{9,11}. It was first demonstrated by Wilkinson *et al.*^{12–14} that local stress values in deformed polycrystal can be unexpectedly high and vary by much as ± 1 GPa. This unusual behavior is the consequence of the $1/r$ type long-range stress field generated by a dislocation. According to the analytical calculations of Groma *et al.*^{15,16} the tail of the probability distribution density of the internal stress generated by a set of straight parallel dislocations decays as

$$P(\sigma) \rightarrow G^2 b^2 C_\sigma < \rho > \frac{1}{\sigma^3} \quad (4)$$

where G is the shear modulus and C_σ (in analogy with XRD) could be called as the *stress contrast factor* since its value depends on the type of dislocation, its line direction and the stress component under consideration¹⁵. Similarly to the X-ray line profile case the tail of the probability distribution is not affected by the actual dislocation arrangement, but only by the average number of dislocations crossing the unit surface. To demonstrate this we took a set of 512 parallel edge dislocations with Burgers vectors parallel to the horizontal axis. Initially the

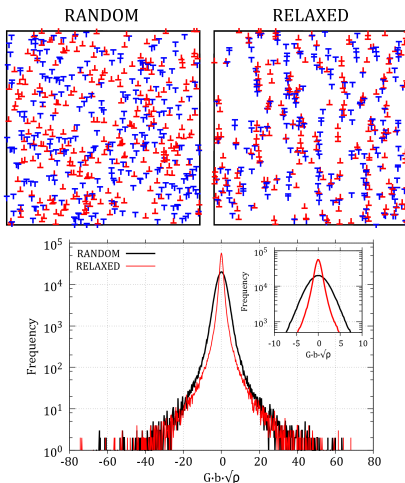


Figure 1: Top boxes: Random and relaxed dislocation configuration. Bottom box: Internal stress distributions obtained on the random (black curve) and the relaxed (red curve) configurations. In the inset the central part of the distributions are enlarged.

dislocations were placed randomly in a square box, then the system was relaxed with an over-damped dynamics¹⁷. For the initial and the relaxed configurations (Fig. 1/(top boxes)) the probability distribution of the shear stress was numerically determined by taking the stress values at 10^6 randomly selected points. As seen in Fig. 1/(bottom box) the tail of the distribution is not affected by the relaxation (in agreement with theoretical predictions^{15,16}),

while the central region of $P(\sigma)$ becomes narrower in the relaxed state (inset in Fig. 1/(bottom box)). It is important to note that for a completely random dislocation distribution the half width of $P(\sigma)$ tends to infinity with the logarithm of the system size, while for the relaxed configuration this divergence is canceled by dislocation-dislocation correlations¹⁵. So, due to stress screening caused by spatial correlations the distribution $P(\sigma)$ becomes independent from the size of the system¹⁵. Similarly to Bragg peak broadening the tail of $P(\sigma)$ is inverse cubic in the asymptotic regime. Hence its second order moment becomes linear in $\ln(\sigma)$ with a slope proportional to the average dislocation density.

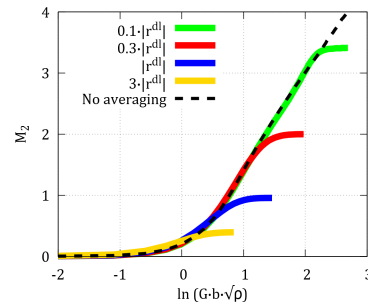


Figure 2: The $M_2(\sigma)$ vs. $\ln(\sigma)$ for 4 different averaging sizes and with no averaging, corresponding to the relaxed configuration shown in Fig. 1.

Due to the finite volume illuminated by the electrons in the SEM, a physically correct interpretation of experimental stress distributions requires averaging the theoretical distributions over the volume illuminated. This introduces a cut-off in the inverse cubic decay of $P(\sigma)$. As a consequence the plot of M_2 versus $\ln(\sigma)$ deviates from the expected linear behavior as demonstrated in Fig. 2 showing the second order restricted moments corresponding to four "spatially averaged distributions" calculated for circles with diameters equal to $0.1r^{dl}$, $0.3r^{dl}$, r^{dl} , and $3r^{dl}$, where r^{dl} is the average dislocation-dislocation distance. The curve with no applied averaging is also shown. As expected the stress level at the cut-off is decreasing with increasing diameter or dislocation density. Therefore, during the evaluation of real data the cut-off introduced by the finite beam size should be considered in the analysis. Since the characteristic linear size of the illuminated volume (of about $10 \times 10 \times 50 \text{ nm}^3$)^{18,19} can be of the same order of magnitude as the average dislocation-dislocation spacing in a heavily deformed metal (of $\approx 30 \text{ nm}$ for a dislocation density of $\approx 10^{15} \text{ m}^{-2}$) the finite beam size could become a limiting factor for the application of the method.

To check the reliability of the EBSD method for dislocation density evaluation subsequent analyses were done by HR-EBSD and XRD on the same crystal surfaces. Cu single crystals of rotated Goss orientation (011)[011] were cut by electrical discharge machining into rectangular cuboid shapes and deformed by channel die compres-

sion up to strain levels of 6% and 10%. The compression was done along the normal direction (ND, parallel to the (011) plane normal), while the sample elongated along the longitudinal direction (LD) ($[0\bar{1}1]$) and was held fixed by the channel walls along the transverse direction (TD). Before deformation and analysis by HR-EBSD and XRD the samples were electro-polished at 15 V for 3 minutes using the Struers D2 electrolyte. The procedure allowed obtaining Kikuchi patterns with the highest image quality.

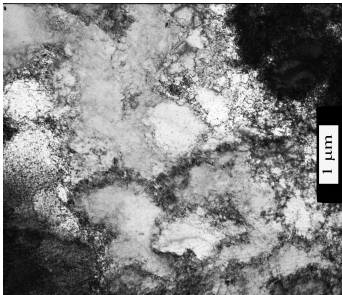


Figure 3: TEM image showing the dislocation cell structure of the crystal deformed up to 6% strain.

The rotated Goss orientation deforms homogeneously in channel die compression. According to the TEM image shown in Fig. 3 a well defined dislocation cell structure develops already at 6% when the cell size is of about $1 \mu\text{m}$. The samples were then characterized by XRD by measuring the 200 line profile on their TD surface. The measurements were done with Cu $K\alpha_1$ radiation in a Panalytical MRD diffractometer equipped with a Bartels primary monochromator and a double bounce analyser, both made of Ge.

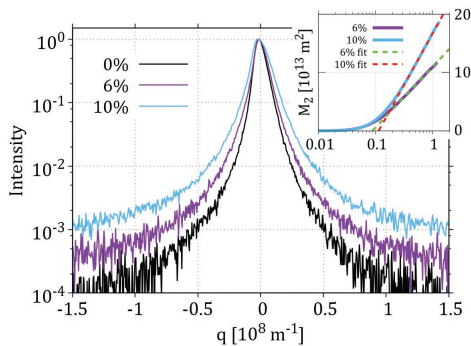


Figure 4: 200 X-ray Bragg peaks corresponding to 0%, 6%, and 10% strain. Inset: The variance M_2 vs. $\ln(q)$ of the peaks measured on deformed samples. The straight lines are fits of the asymptotic regime.

The 200 peaks and their variances $M_2(q)$ versus $\ln(q)$ are shown in Figs. 4 and 4/(Inset), respectively. The dislocation density is directly obtained from the slope of the lines fitted to the asymptotic regime. The results given in the second column of Table 1 were obtained using

a diffraction contrast factor $C_g = 0.397$ corresponding to an equal dislocation population in each slip system.

strain	ρ_{XRD}	ρ_{EBSD}
6%	$7.3 \cdot 10^{14} \text{m}^{-2}$	$2.3 \cdot 10^{14} \text{m}^{-2}$
10%	$1.2 \cdot 10^{15} \text{m}^{-2}$	$1.3 \cdot 10^{15} \text{m}^{-2}$

Table I: Dislocation densities obtained by X-ray line profile analysis and HR-EBSD.

The EBSD scans were done with a step size of 100 nm on a square grid covering an area about $25 \mu\text{m} \times 30 \mu\text{m}$. The backscattered Kikuchi patterns were recorded with a NordlysNano detector of 1344×1024 pixels. The acquisition was monitored with the AztecHKL software, which was also used to calculate the pattern centers necessary for performing the high-resolution evaluation. The stress at each measurement point was determined with the cross-correlation method of Kikuchi patterns developed by Wilkinson *et al.*¹¹. Since the scanned area is much larger than the characteristic size of the microstructure (dislocation cells with a size of about $1 \mu\text{m}$, see Fig. 3), the probability distribution of internal stresses can be considered a macroscopic quantity characterizing the structure.

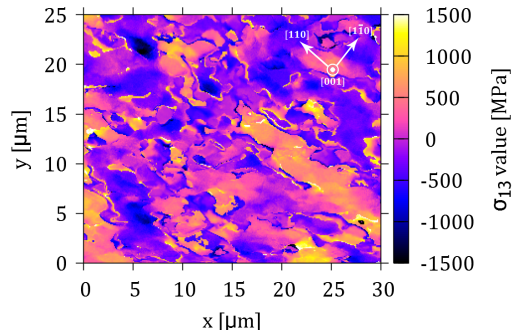


Figure 5: The σ_{13} stress component map obtained by HR-EBSD on the Cu single crystal compressed to 6% strain. The stress levels indicated are relative values to the stress level at the center of the area scanned.

The σ_{13} stress component map obtained on the sample with 6% strain is plotted in Fig. 5. In agreement with the TEM image (Fig. 3), the cell structure with typical cell size of $1 \mu\text{m}$ is seen with long range internal stress develops in the cell interiors². A detailed analysis of the long range stress is out of the scope of the present paper, it will be published elsewhere.

The probability distributions of the σ_{13} stress component characterizing the undeformed and deformed samples are plotted in Fig. 6. $P(\sigma_{13})$ is very narrow for the undeformed sample and it broadens with increasing deformation. Remarkably, the tails of $P(\sigma_{13})$ extend outside values as large as ± 1 GPa. Similar behavior was first reported by Wilkinson *et al.* on deformed polycrystalline Cu and ferritic steel¹⁴. Since one can clearly identify a

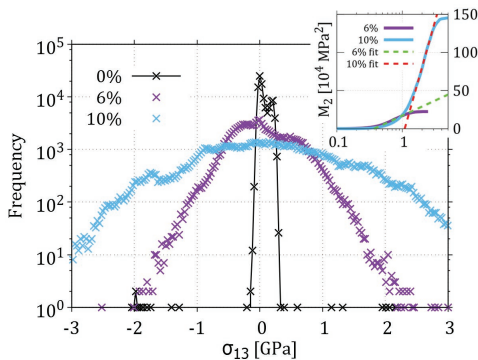


Figure 6: a) The probability distribution of the σ_{13} stress component at strains of 0%, 6% and 10%. Inset: The corresponding variances M_2 versus $\ln(q)$ for the deformed samples, with the straight lines fitted in the asymptotic regime.

linear regime on the M_2 versus $\ln(\sigma_{13})$ plots (Fig. 6/(Inset)) the broadening of $P(\sigma_{13})$ can only be caused by the presence of dislocations (other type of stress source would generate different decay in the tail part¹⁵). This reasoning is also supported by the rather narrow $P(\sigma_{13})$ distribution corresponding to the undeformed sample. For stress values larger than about 2 GPa the second order restricted moments clearly deviate from the linear dependence in $\ln(\sigma_{13})$. As discussed above this is the consequence of the measuring setup and related to the unavoidable averaging over the volume illuminated by the electron beam. Nevertheless, the linear regime can be well identified on the plots presented. (The cut-off is certainly absent on the variance of the X-ray peaks.) According to Fig. 2 the linear region disappears when the size of the averaging zone equals the mean dislocation-dislocation spacing. This imposes an instrumental limit in the application of the method for heavily deformed samples.

According to Eq. (4) the slope of the line fitted in the asymptotic regime is proportional to the total dislocation density. Its determination requires the knowledge of the *stress contrast factor* C_σ in Eq. (4), which can be calculated according to Refs.^{15,16}. For the stress component σ_{ij} considered in the analysis one has to evaluate the integral:

$$C_{ij} = \frac{1}{G^2 b^2} \int_0^{2\pi} [r \sigma_{ij}^{\text{ind}}(r, \varphi)]^2 d\varphi \quad (5)$$

where σ_{ij}^{ind} is the stress generated by a dislocation with a given line direction \vec{l} and Burgers vector \vec{b} in the xy plane of the coordinate system in which the stress tensor is calculated during the evaluation of the Kikuchi patterns. In Eq. (5) (r, φ) denotes the polar coordinates in the xy plane. (Due to the $1/r$ type of decay of the stress field generated by a dislocation, the integral is independent from r .) Since in anisotropic materials the stress field of a straight dislocation cannot be always given in a closed

analytical form²⁰ C_σ can only be calculated numerically. Moreover, since in most cases dislocations of different types and line directions can exist in the same structure, one has to calculate the appropriate weighted average of C_σ corresponding to given \vec{b} and \vec{l} . This issue is out of the scope of this paper. For simplicity we use the value corresponding to an edge dislocation with line direction perpendicular to the sample surface. In this case $C_\sigma = 1/(8\pi(1-\nu)^2)$ where ν is the Poisson number¹⁵.

The dislocation densities of the deformed samples are summarized in the third column of Table 1. The ρ_{EBSD} values given correspond to the average values obtained from the stress components σ_{13} , σ_{22} , and σ_{23} . (Due to the deformation geometry applied the other two stress components σ_{11} , and σ_{12} are much smaller with much larger error, so they were not taken into account.) By comparing them to the values obtained from XRD (column 2) one can conclude that there is a good agreement between the results of the two methods. At 10% strain the difference is within a few % of relative error, while at 6% strain the HR-EBSD gave smaller ρ than the XRD by about a factor of 3. The last difference can be attributed first of all to the influence of the larger dislocation cell size at 6% strain resulting that the volume scanned during the EBSD measurement may not large enough to give a representative mean value for the dislocation density. Another reason for the difference can be a change in the main dislocation character and the population of different slip systems with increasing strain. It seems to be that the C_σ used is not really relevant for the 6% strain case. The issue requires further detailed investigations.

It is remarkable, however, that the assumption considering edge dislocations only gave good agreement with XRD results at 10% strain. This emphasizes the strong physical basis of the evaluation method proposed. For more accurate dislocation density values a TEM analysis of prevailing dislocation types and line vectors is inevitable both for the XRD and HR-EBSD methods

Summing up: HR-EBSD was traditionally used to determine the *geometrically necessary dislocation density*²¹. With the analysis of the tail of the stress probability-distribution function obtained from HR-EBSD the stored, *total dislocation density* present in the sample can also be determined. This opens new perspectives for the application of EBSD in determining *mesoscale* parameters in a heterogeneous sample, such as a polycrystal.

The authors acknowledge insightful discussion with Prof. Claire Maurice (Ecole Nationale Supérieure des Mines, Saint-Etienne, France). This work was supported by the French-Hungarian collaboration BALATON, the Hungarian Scientific Research Fund (OTKA) under contract numbers K-105335 and PD-105256, and the European Commission under grant agreement No. CIG-321842. PDI was supported by the János Bolyai Scholarship of the Hungarian Academy of Sciences.

-
- * Electronic address: groma@metal.elte.hu
- ¹ H. Mughrabi and T. Ungar, *Dislocations in Solids, Vol. 11* (2002).
 - ² T. Ungar, H. Mughrabi, D. Rönnpagel, and M. Wilkens, *Acta Metall.* **32**, 333 (1984).
 - ³ G. I. Taylor, Proceedings of the Royal Society of London A: Mathematical, Physical and Engineering Sciences **145**, 362 (1934), ISSN 0950-1207.
 - ⁴ A. Wilkinson, E. Clarke, T. Britton, P. Littlewood, and P. Karamched, *The Journal of Strain Analysis for Engineering Design* **45**, 365 (2010).
 - ⁵ I. Groma, *Phys. Rev. B* **57**, 7535 (1998).
 - ⁶ F. Székely, I. Groma, and J. Lendvai, *Phys. Rev. B* **62**, 3093 (2000).
 - ⁷ A. Borbély and I. Groma, *Appl. Phys. Letters* **79**, 1772 (2001).
 - ⁸ I. Groma, D. Tüzes, and P. Ispánovity, *Scripta Mater.* **68**, 755 (2013).
 - ⁹ A. J. Wilkinson, G. Meaden, and D. J. Dingley, *Ultramicroscopy* **106**, 307 (2006).
 - ¹⁰ A. Wilkinson, T. Britton, J. Jiang, G. Meaden, and D. Dingley, *Microscopy and Microanalysis* **17**, 402 (2011).
 - ¹¹ T. Britton and A. Wilkinson, *Ultramicroscopy* **114**, 82 (2012).
 - ¹² J. Jiang, T. B. Britton, and A. J. Wilkinson, *Acta Mater.* **61**, 5895 (2013).
 - ¹³ J. Jiang, T. B. Britton, and A. J. Wilkinson, *Acta Mater.* **94**, 193 (2015).
 - ¹⁴ A. J. Wilkinson, E. Tarleton, A. Vilalta-Clemente, J. Jiang, T. B. Britton, and D. M. Collins, *Appl. Phys. Letters* **105**, 181907 (2014).
 - ¹⁵ I. Groma and B. Bakó, *Phys. Rev. B* **58**, 2969 (1998).
 - ¹⁶ F. F. Csikor and I. Groma, *Phys. Rev. B* **70**, 064106 (2004).
 - ¹⁷ P. D. Ispánovity, I. Groma, G. Györgyi, F. F. Csikor, and D. Weygand, *Phys. Rev. Letters* **105**, 085503 (2010).
 - ¹⁸ N. Yao and Z. Wang, *Handbook of Microscopy for Nanotechnology*, Nanostructure Science and Technology Series (Springer US, 2006), ISBN 9781402080067.
 - ¹⁹ D. Chen, J. Kuo, and W. Wu, *Ultramicroscopy* **111**, 1488 (2011), ISSN 0304-3991.
 - ²⁰ J. W. Steeds, *Introduction to anisotropic elasticity theory of dislocations* (Clarendon Pr., 1973).
 - ²¹ A. J. Wilkinson and D. Randman, *Phil. Mag.* **90**, 1159 (2010).